Integrative and Comparative Biology

Integrative and Comparative Biology, volume 58, number 4, pp. 703–711
doi:10.1093/icb/icy014

Society for Integrative and Comparative Biology

SYMPOSIUM

On the Hydrodynamics of *Anomalocaris* Tail Fins

K. A. Sheppard,[*] D. E. Rival[*] and J.-B. Caron[1,†,‡,§]

[*]Department of Mechanical and Materials Engineering, Queen's University, Kingston, Ontario, Canada ON K7L;
[†]Department of Natural History (Palaeobiology Section), Royal Ontario Museum, Toronto, Ontario, Canada M5S 2C6;
[‡]Department of Ecology and Evolutionary Biology, University of Toronto, Toronto, Ontario, Canada M5S 3B2;
[§]Department of Earth Sciences, University of Toronto, Toronto, Ontario, Canada M5S 3B1

From the symposium "From Small and Squishy to Big and Armored: Genomic, Ecological and Paleontological Insights into the Early Evolution of Animals" presented at the annual meeting of the Society for Integrative and Comparative Biology, January 3–7, 2018 at San Francisco, California.

[1]E-mail: jcaron@rom.on.ca

Synopsis *Anomalocaris canadensis*, a soft-bodied stem-group arthropod from the Burgess Shale, is considered the largest predator of the Cambrian period. Thanks to a series of lateral flexible lobes along its dorso-ventrally compressed body, it is generally regarded as an efficient swimmer, well-adapted to its predatory lifestyle. Previous theoretical hydrodynamic simulations have suggested a possible optimum in swimming performance when the lateral lobes performed as a single undulatory lateral fin, comparable to the pectoral fins in skates and rays. However, the role of the unusual fan-like tail of *Anomalocaris* has not been previously explored. Swimming efficiency and maneuverability deduced from direct hydrodynamic analysis are here studied in a towing tank facility using a three-vane physical model designed as an abstraction of the tail fin. Through direct force measurements, it was found that the model exhibited a region of steady-state lift and drag enhancement at angles of attack greater than 25° when compared with a triangular-shaped reference model. This would suggest that the resultant normal force on the tail fin of *Anomalocaris* made it well-suited for turning maneuvers, giving it the ability to turn quickly and through small radii of curvature. These results are consistent with an active predatory lifestyle, although detailed kinematic studies integrating the full organism, including the lateral lobes, would be required to test the effect of the tail fin on overall swimming performance. This study also highlights a possible example of evolutionary convergence between the tails of *Anomalocaris* and birds, which, in both cases, are well-adapted to efficient turning maneuvers.

Introduction

The primitive soft-bodied arthropod *Anomalocaris canadensis*, initially known from the middle Cambrian Burgess Shale of British Columbia (Briggs 1979), is considered the apex predator of the Cambrian period, with large adult specimens estimated to reach half a meter in length (Whittington and Briggs 1985). A predatory habit is suggested by its ventral mouth cone, equipped with teeth projecting inwards (Daley and Bergström 2012), its prominent dorsolateral camera-type eyes on stalks—presumably with large number of ommatidia (based on a potentially related species from Australia), suggesting acute vision (Paterson et al. 2011), a pair of frontal grasping appendages with strong serrated spines (Briggs 1979), and a series of flexible lateral lobes along its dorso-ventrally flattened body with a terminal tripartite tail fin supposedly well-adapted for swimming (Whittington and Briggs 1985). Although speculative, additional indirect evidence of a predatory mode of life includes bite marks on trilobites and presumed anomalocaridid coproliths (Nedin 1999). Thanks to new specimens recovered by the Royal Ontario Museum (Collins 1996), recent studies (Daley and Bergström 2012; Daley and Edgecombe 2014), and new observations, the overall appearance of *A. canadensis* can now be reconstructed more accurately (Fig. 1B). The tail fin, which is central to the present study, consists of three imbricated pairs of vanes with the longest one most distant from the body axis, and the shortest and also most posterior one, nearest to the body axis. The vanes were

Advance Access publication April 25, 2018

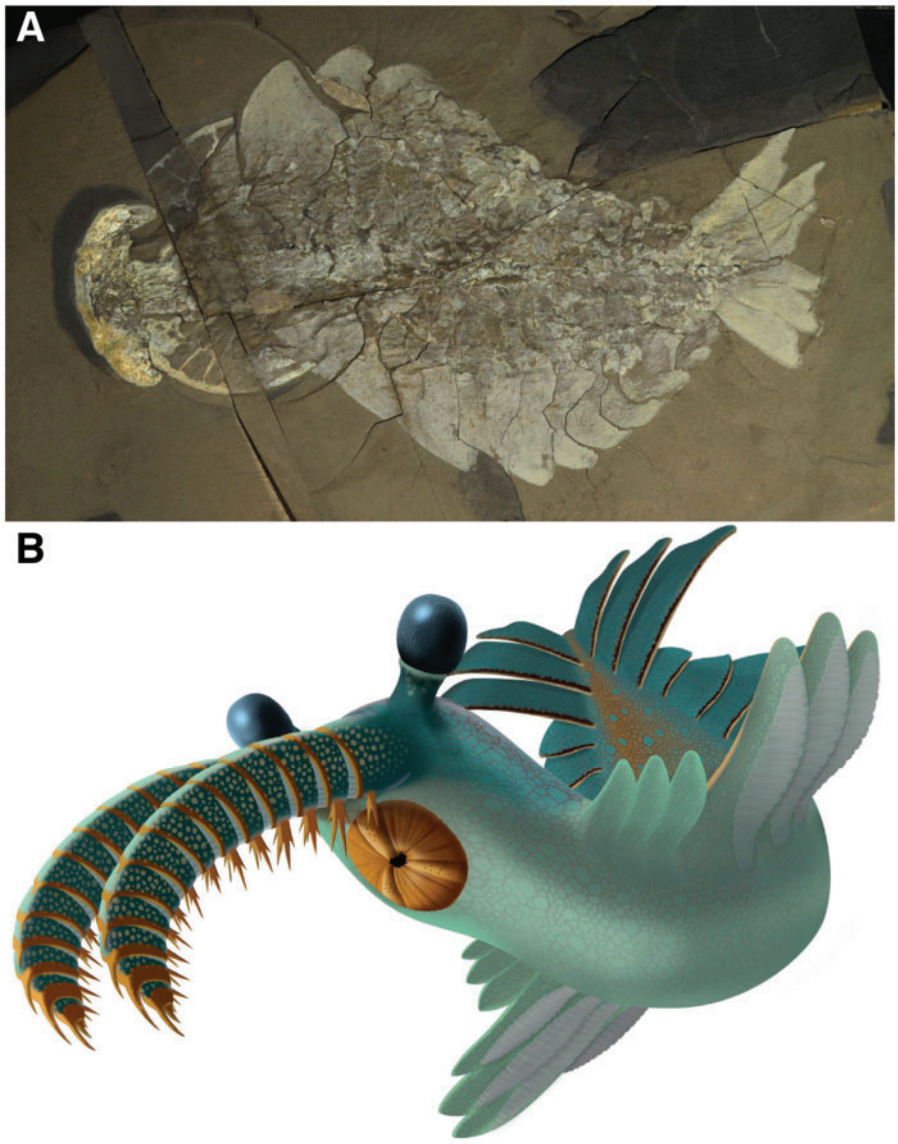

Fig. 1 *Anomalocaris canadensis* from the middle Cambrian Burgess Shale. (**A**) Complete specimen, showing posterior tail fin to the right, ROMIP 51211. (**B**) Full reconstruction with new morphological interpretations based on recent studies (in particular, Daley and Bergström [2012] and Daley and Edgecombe [2014]), and personal observations (J.-B.C.). Drawing by Marianne Collins © Royal Ontario Museum.

originally reconstructed to be dorsal and oblique to the rest of the body (Collins 1996); however, more recent interpretations suggest that the tail fin vanes extended along the lateral margins of the body at a slight dorsal angle (Daley and Edgecombe 2014), also consistent with our own observations (Fig. 1B). The degree of dorsoventral flexibility of the tail is difficult to assess, although in all specimens with tail fins preserved, the vanes seem relatively rigid compared with the associated lateral lobes. The vanes are never fully bent along their lengths and also seem to maintain relatively stable positions relative to each other, even when the rest of the body is twisted or shows a degree of decay and disarticulation.

Morphologically, *A. canadensis* shares broad similarities of at least parts of its external anatomy with a number of evolutionarily unrelated modern swimmers, which in principle should provide some insights into the likely functionality of its lateral lobes and the contribution of its unique tail fin in locomotion. In terms of its swimming mode, *A. canadensis* has previously been compared to rays in studies using theoretical hydrodynamic simulations (Usami et al. 1998, 2003; Usami 2006). In these studies, optimal swimming performance was found to occur when the lateral overlapping lobes acted as a single flap, as in many batoid fishes. Batoid fishes use a combination of undulatory and oscillatory

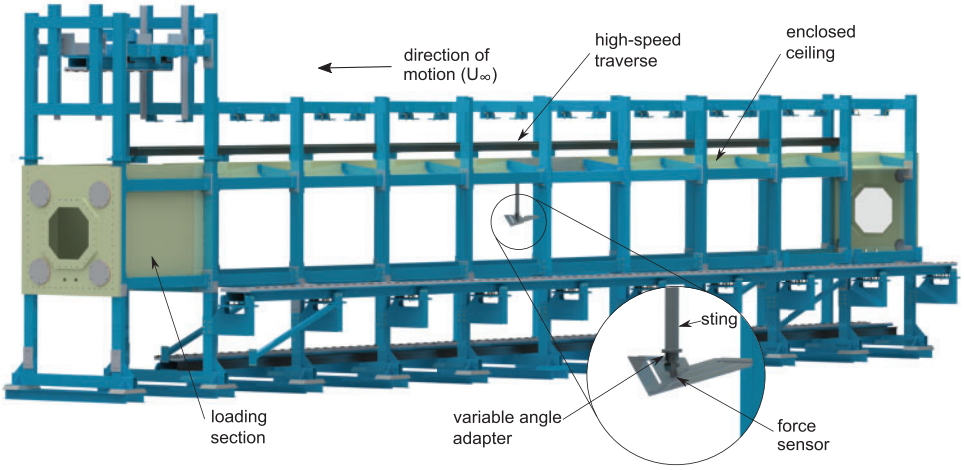

Fig. 2 Schematic of the optical towing tank used for direct force measurements. The model is attached to a streamlined fixture (or sting) that connects the model to the support structure and is towed upside-down from right to left in the figure. A force sensor is attached to the model surface at its geometric center.

(flapping) movements, using both axial-based and pectoral-fin based locomotion (Rosenberger 2001), although the relative role of undulatory versus oscillatory movements in *A. canadensis* and how it propelled itself either with its body and tail or with its expanded lateral lobes are questions that have yet to be explored.

While the swimming efficiency of its flexible lateral lobes may be important to fully categorize the swimming characteristics of *A. canadensis*, information regarding its ability to rapidly change direction and to perform bursting maneuvers from rest, thanks to its unique tail morphology, may prove beneficial in informing understanding of its possible predatory habits. The maneuverability of an animal may be associated with the performance of rapid escape maneuvers, steady turning maneuvers, and by maintaining stability when perturbations are present in the flow (Webb 2006). Due to its unique morphology, the tail fin of *A. canadensis* was selected as a focus for a general hydrodynamic analysis to provide information regarding the theoretical motion for which it was likely most adept and where the tail–fin geometry—informed by new paleontological knowledge—may indicate a compromise among multiple functions. Additionally, the results from a hydrodynamic analysis may provide insight as to the relative swimming strength of *A. canadensis* in both steady and unsteady (acceleratory) propulsion. Maintaining the view that *A. canadensis* was an apex predator and therefore a probable powerful and highly maneuverable swimmer, it is hypothesized that the primary purpose of the tail fin was to augment the resultant normal force in both unsteady escape maneuvers and rapid changes in direction.

Experimental methods

All experiments were conducted in a towing tank facility at Queen's University, Ontario, Canada, with a square cross-sectional area of 1 m^2 and a total traverse length of 15 m (Fig. 2)—the geometry of the tail fin abstraction is examined in further detail in the section "Physical tail fin abstraction." The towing tank has five sides of optical access and a full cover on the ceiling to reduce free-surface effects. Accounting for the loading section and buffer region, the general motion of the model consisted of an acceleration from rest, a period of steady motion, and deceleration to rest over a total length of 11.5 m. A steady towing velocity of 1 m/s was selected to yield Re = 300,000 based on the mid-span chord of the model. This Reynolds number was chosen to be representative of *A. canadensis* swimming and is discussed further in the section "Selection of parameters." The effect of blockage (the ratio between the frontal projected area of the model and the cross-sectional area of the tank) is considered negligible, with a maximum value of 6.4% for an angle of attack of 45°, denoted as α in Fig. 4.

Physical tail fin abstraction

Most simply, the tail fin, which is comprised of three pairs of imbricated vanes, can be represented from a dorsal point of view as a triangle (Fig. 1A)—termed a delta wing in aerodynamics. The vanes are separated by gaps, which are parallel to the leading edges, resulting in a shape resembling a series of chevrons. For the purposes of the current study, the three pairs of vanes are considered to lie on a common plane with equally-spaced gaps between each of the vanes

and straight trailing edges. (Fossils show vanes with irregular trailing edge profiles [Fig. 3], which were not recreated in this study, in order to reduce the number of potential confounding effects). While a geometry considering a variable angle between each of the vanes and the horizontal plane may have the potential to influence the swimming performance, the basic abstraction considered here enforces a planar geometry. Three pairs of chevron-shaped pieces were constructed of 3.175 mm-thick stainless steel for strength and corrosion resistance. These were mounted to a central bar connected to the towing tank traverse (Fig. 4). A plain triangular reference model was constructed using the same overall dimensions, material, and mode of attachment as in the chevron-shaped model, to specifically test whether or not the gaps between vanes had any hydrodynamic effects. In early testing iterations, the chevron pieces were observed to bend significantly away from the common plane when loaded. As a result, two additional support bars (Fig. 4) were added to the trailing edge to minimize this effect and ensure a consistent testing geometry across all angles of attack. Due to the relatively high angles of attack being tested, the flow is expected to be largely separated, with the trailing edge supports having minimal effect on the flow. In reality, the gaps between vanes would have been highly variable during a propulsive stroke. Minimal gap variations would be expected near the body, but much greater gaps would be expected more distally due to the relatively flexible nature of the vanes. The effects of vane flexibility were beyond the scope of this study and require further investigation.

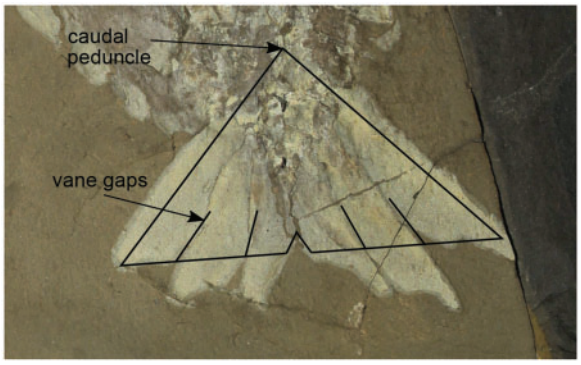

Fig. 3 Tail fin preservation of *A. canadensis* specimen ROMIP 51211 showing the vanes and general shape of the region of interest.

Selection of parameters

While the exact maximal size and swimming speed of *A. canadensis* are unknown, the Reynolds number regime and angles of attack are hypothesized to be broadly comparable to what we know applies in fishes. A flow can be characterized by its Reynolds number:

$$\mathrm{Re} = \frac{U_\infty c}{\nu},$$

where U_∞ is the flow velocity, c is a characteristic mid-span chord length, and ν is the kinematic viscosity of the fluid. As described by Sfakiotakis et al. (1999), a typical adult fish swims in a Reynolds number regime ranging from 10^3 to 10^6. Webb (1975) divides swimming speed into three different categories: "cruising or sustained," "prolonged or steady," and "sprint or burst." Fishes do not swim entirely within a single range of speeds, and instead modulate their speeds based on the desired activity level. To account for size, swimming speeds are often presented with units of body lengths per second (BL/s). The Atlantic tuna, which is considered a fast swimmer, can attain maximal swimming speeds up to 9.3 BL/s (Videler and Wardle 1991). In dorsoventrally flattened fish, which are more similar in

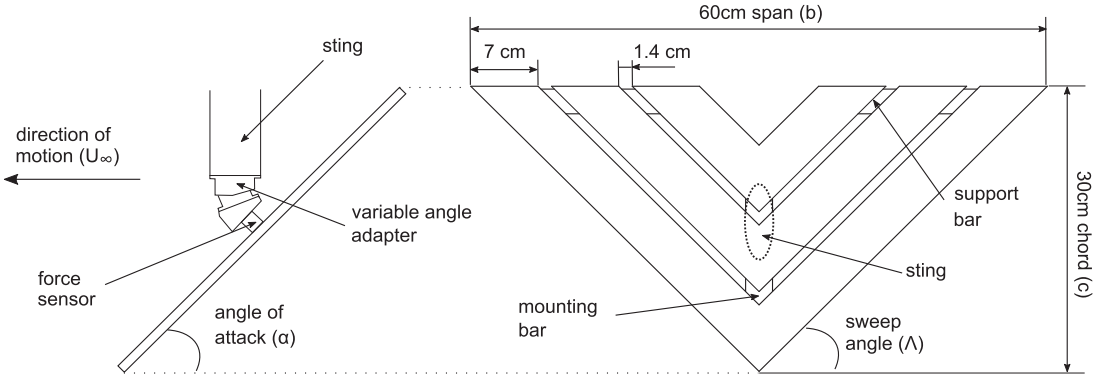

Fig. 4 Schematic of the chevron model and connection to the towing tank traverse via a fixture (sting, see also Fig. 2). The model is towed from right to left by the traverse after setting a desired angle of attack on a variable adapter. An identical mounting setup is used for the triangular flat plate used as a base testing case. The angle of attack can be varied from 5° to 45° and the sweep angle is 45°.

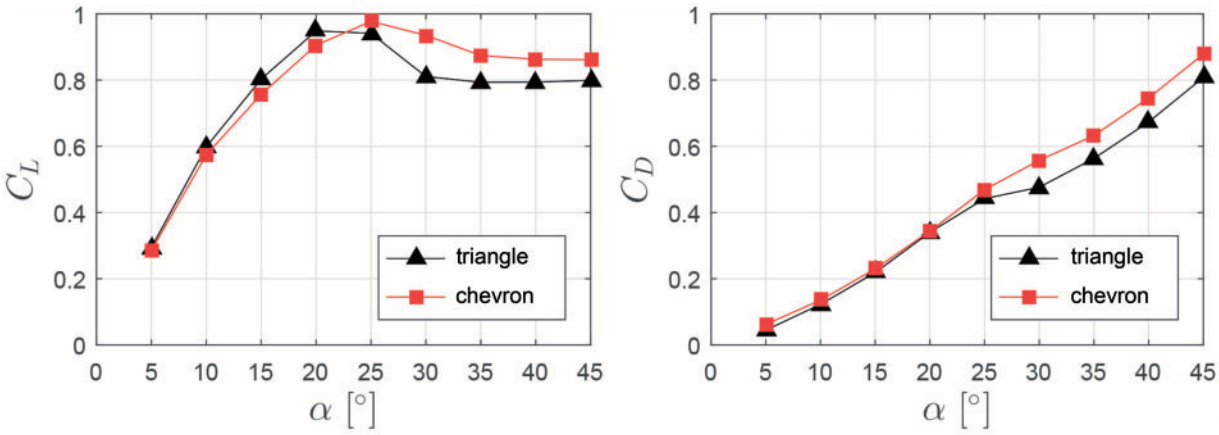

Fig. 5 Average steady-state lift and drag coefficients for triangular and chevron models shown in black and red, respectively, as a function of angle of attack. For angles of attack greater than 25°, an enhancement in force is observed, although at low angles, the differences are insubstantial.

overall shape to *A. canadensis*, the maximal speed is typically much lower, in the order of ca. 1–3 BL/s (Di Santo et al. 2017).

Selecting a swimming speed of 3 BL/s as a conservative estimate for *A. canadensis*, and approximating the tail length as 15% of the body length to match the proportion of the best-preserved specimen (Fig. 1A), albeit smaller specimens might show different proportions (Daley and Edgecombe 2014), yields $\mathrm{Re} \approx 450{,}000$. Considering the optimal range of the force transducer for a favorable signal-to-noise ratio, as well as the capabilities of the testing facility, $\mathrm{Re} = 300{,}000$ was selected for a model with a 30 cm mid-span chord length.

Direct force measurements

A submersible, six-component ATI-Nano force sensor was mounted to the geometric center point on the pressure side of the triangular and chevron models. Forces were measured at a sampling rate of 1000 Hz with a resolution varying from 1/24 N to 1/8 N, depending on the axis of interest. The general motion consisted of an acceleration from rest, a period of steady-state travel, followed by a return to rest at 11.5 m traveled. Force data were recorded for angles of attack ranging from 5° to 45° to observe the steady-state performance of the model after reaching a constant velocity. Average force and moment coefficients were then calculated over a period of 2 s during the constant velocity portion of the prescribed motion. Uncertainties calculated for the steady-state lift and drag coefficients are on the order of 10^{-4} for $N = 6000$ independent data points, which is representative of the standard deviation of the data. While the true uncertainty in the measurement is expected to be higher due to the partial dependence of samples, error bars in Fig. 5 are on the order of the symbol sizes (Figliola and Beasley 2011). At steady-state, average values are calculated over a range of 2 s with three runs for each set of parameters. Three runs per angle of attack were recorded to compute an average of several thousand points under steady-state conditions. The steady-state lift and drag are being considered as measures of the animal's ability to rotate the center of mass of its body using the force generated on the tail, as is done in a banking turn or change of direction, defined here as a steady maneuver. Force measurements were conducted for angles of attack ranging from 5° to 45° for both the triangular and chevron models (Fig. 5). A single angle of attack of interest was then selected based on the results of initial force testing to further elucidate the unsteady hydrodynamic performance during the initial acceleration from rest. This highly acceleratory motion may be compared with maneuvers such as an escape from a resting start or a propulsive motion. The rate of initial acceleration from rest is characterized by the parameter:

$$a^* = \frac{U_\infty^2}{2ac},$$

where a is the dimensional acceleration, U_∞ is the towing velocity of 1 m/s, and c is the mid-span chord length. The force measurement system used in the current work has been verified in a previous study by Fernando and Rival (2016) on the flow characteristics of flat plate abstractions of common natural propulsors.

For all subsequent force analyses, the parameters of interest are the lift, drag, and moment coefficients—normalized by the dynamic pressure and the planform area of each model. The lifting force is the resultant force normal to the direction of motion, and the drag force is the resultant parallel and opposite to the direction of travel. The lift and drag may be combined to give an overall normal force, a parameter necessary to provide a turning moment at the body's center of gravity. The pitching moment is a measure of the tendency of the model to return to a neutral state about the quarter-chord position, and may be important in characterizing the input energy in actuating the tail. The sign of the pitching moment indicates the direction of natural rotation of the model, either toward or away from a neutral position.

Results

For low angles of attack, differences between the chevron and plain models in lift and drag coefficients were limited (Fig. 5); however, at angles greater than 25°, an enhancement in lift of up to 15.3% at 30° is observed. The drag coefficient of the chevron model was found to have a maximum increase of 17.0% for an angle of attack of 30°. Analyses with the steady-state moment coefficient measured about the quarter-chord position (Fig. 6) show that, for angles greater than 25°, the chevron model experiences an enhancement in average magnitude. The maximum percent increase in the magnitude of the pitching moment for the chevron model over the triangular plate measured was 10.8% for an angle of attack of 30°. Noting that the most significant steady-state differences between the two models were observed at an angle of attack of 30°, force testing was conducted for a range of acceleration rates at this angle. The negative *y*-axis indicates that the moment was nose-down, as expected from the literature for delta wings comparable to the shape used in the current study (Gursul et al. 2005).

During the transient force peak associated with the acceleration from rest, the two models performed similarly and the force enhancement measured at steady-state conditions was not observed (Fig. 7). At this angle of attack, the overall force magnitude measured for the triangular flat plate is slightly higher in the transient region of the motion, indicating that the chevron shape does not give a significant benefit in highly acceleratory motions. While the chevron model does not provide a benefit in the acceleratory region of the motion, the gaps do not significantly hinder the generation of lift during steady-state motions.

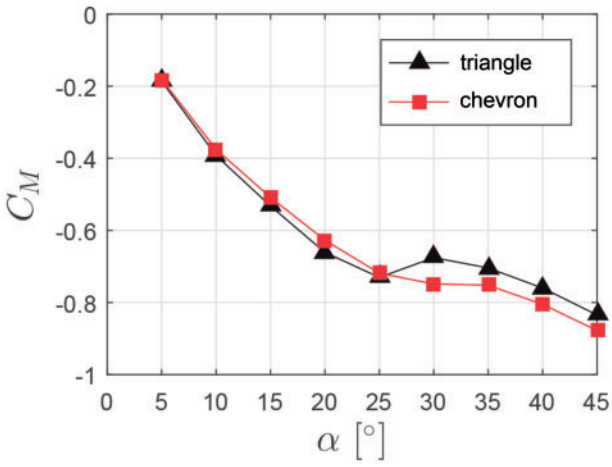

Fig. 6 Average steady-state moment coefficient measured at the mid-chord position and translated to a quarter-chord position as a function of angle of attack. For angles of attack greater than 25°, an enhancement in magnitude is observed for the chevron model, although differences are less pronounced than for measured lift and drag coefficients. At low angles of attack, differences between the two models are significantly reduced. The negative axis corresponds to a nose-down pitching moment.

The response of the drag coefficient at this angle is similar, although with a lower overall magnitude due to the calculation of the resultant force from the components measured. The resulting nose-down pitching moment coefficient translated to a quarter-chord position was found to exhibit an increase in magnitude at steady-state.

Discussion

The results of the current study suggest that the geometry of the tail fin of *A. canadensis* provides a hydrodynamic benefit in performing maneuvers such as banking turns or rapid changes in direction due to the enhanced normal force relative to a solid triangular shape without structured vanes. As a comparison, in fish, the normal force on the tail fin is used to assist in providing a turning moment for the body, while a centripetal force is required to turn the center of mass of the animal (Fig. 8). A small turning radius and therefore a large normal force indicates some benefit in maneuverability. The same concept can be applied to *A. canadensis* by considering maneuvers in the vertical plane or by applying an additional rolling motion to the body. In these rapid maneuvers, the normal force is of more importance than either the lift or drag alone, indicating that the increase in drag is a benefit rather than a hindrance as in many traditional aerodynamic problems where low drag is desired.

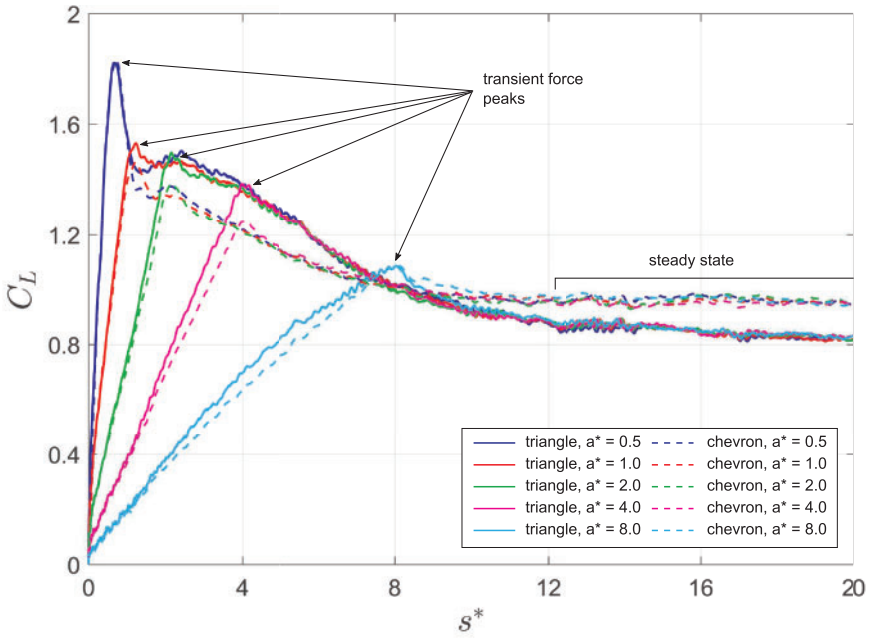

Fig. 7 Normalized resultant force perpendicular to the direction of motion for an angle of attack of 30° and a range of initial acceleration rates as a function of s^* (the distance traveled normalized by the mid-span chord). Two distinct regions are observed: acceleration and subsequent relaxation, and steady-state, where the slotted model denoted by dashed lines is observed to give a significant increase in steady-state lift for all acceleration values tested.

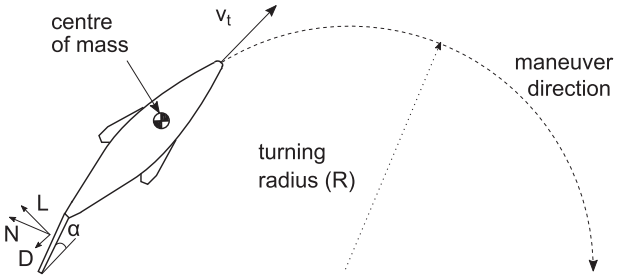

Fig. 8 Schematic of turning maneuver for a generic fish shape. The tangential velocity of the fish is given by ν_t. The resultant normal force on the tail fin (N) is used to provide a turning moment and assist with turning the center of mass of the fish.

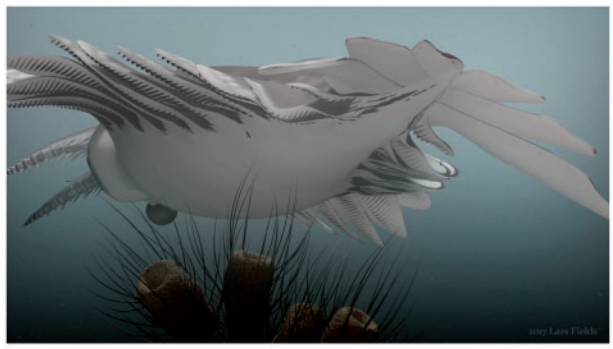

Fig. 9 Hypothetical reconstruction of the swimming behavior of *A. canadensis*. Model (see movie file in Supplementary data) by Lars Fields © Royal Ontario Museum.

Due to the high-lift characteristics of the tail–fin abstraction, it is believed that the ideal function of the tail fin is primarily associated with swimming maneuverability, although the results did not indicate that the shape would make for an ineffective propulsor (see Fig. 9 and the Supplementary data video for a reconstruction of *A. canadensis* and its likely swimming mode). The gaps between vanes enhanced performance at steady-state, and did not significantly hinder lift production in acceleratory motions. As there was no observed benefit from the gaps in the acceleratory region, the results suggest that, to maximize performance, the vanes may have been forced together under loading during propulsive strokes in order to provide more of a planar surface. The enhanced steady-state normal force associated with the tail fin may provide a benefit in maneuverability not available to modern rajiform swimmers with little to no tail fin. While the lateral lobes of *A. canadensis* were likely used for active propulsion through undulating motions, the force enhancement on the tail–fin abstraction suggests that the geometry of the tail fin was well-suited to providing a large turning moment.

More generally, the tail fin of *A. canadensis* and possibly *A. saron* from China (Hou et al. 1995) has

parallels in both morphology, and probably overall function, with bird tails. While bird tails can be observed in many shapes and sizes, one specific function they all share is to augment lift during acceleration and turning maneuvers (Thomas 1997). A portion of the lift generated at the tail can then be used to turn the body by positioning the tail in the direction of desired acceleration. The tail of a bird is considered essential to maintaining stability during the performance of maneuvers (Tobalske 2007). A study on the maneuvering flight of a steppe eagle, *Aquila nipalensis*, found that the spread and angle of the tail was consistent across all measured banking turns, and assisted with providing the nose-down moment necessary to perform the maneuver (Gillies et al. 2011). In many species, the general triangular shape of bird tails can be compared with delta wings, triangular lifting surfaces also exemplified by the general shape of *Anomalocaris* tail fins (Thomas 1993). Bird tails serve as effective control surfaces and assist with the performance of turning and perching maneuvers. Although obviously adapted to different environments, the vane-like structure of the *Anomalocaris* tail fin can be broadly compared from an engineering perspective with the swept feather positioning of many bird tails, where the ability to spread feathers and create gaps may result in similar performance enhancements (to be tested in the future).

Conclusions

The unique fan-like tail of *A. canadensis* was subject to hydrodynamic analysis. A model comprising three chevron shapes was constructed of stainless steel and compared with a flat triangular plate to observe the effect of the multi-vane geometry. Average steady-state forces generated on each of the models were measured and compared for a range of angles of attack. An enhancement in measured lift and drag was observed, in particular for moderate-to-high angles of attack. This result was most prominent for an angle of attack greater than 25°. Five different rates of acceleration were investigated and the accelleratory response of the two models was compared. The two models showed little difference as large force peaks were observed for each, although the triangular model showed a small improvement in lift generation over the chevron model.

While the lateral lobes of *A. canadensis* were likely used for undulatory locomotion, the specific function of the tail fin and its effect on overall propulsion would require further studies. Our results suggest, however, that the multi-component tail fin shape of *A. canadensis* provided a benefit in generating a large normal force on the tail used for maneuvers, but did not improve performance in propulsive motions. This is not to say that the tail fin geometry would not have made for an effective propulsor, as in many species of fish, but we conclude that the unique shape is primarily of benefit to turning performance. The overall tail–fin function of *A. canadensis* can be compared with the lift augmentation and maneuver control often provided by bird tails. Similarities in shape and structure of the vanes with tail feathers indicate a possible evolutionary convergence in high-performance propulsion, whether through water or air.

Acknowledgments

We thank two anonymous reviewers for their constructive remarks, J. Fernando, M. Marzanek, and C. Bond for assistance with data collection and processing, Marianne Collins for illustrations (Fig. 1B), Lars Fields for animations (Fig. 9; Supplementary data), and Sara Scharf for editorial suggestions.

Funding

The current work was part of K.A.S.'s MASc thesis at Queen's University. K.A.S. and J.-B.C. thank Erik Sperling and Kevin Kocot, for their invitation to present at their SICB 2018 symposium titled: "From Small and Squishy to Big and Armored: Genomic, Ecological and Paleontological Insights into the Early Evolution of Animals." J.-B.C. also thanks the Paleontological Society for a travel grant. D.E.R. research was supported by an NSERC Discovery [grant 401927]. J.-B.C. research was supported by an NSERC Discovery [grant 341944]. This is Royal Ontario Museum Burgess Shale Research Project No. 77.

Supplementary data

Supplementary data available at *ICB* online.

References

Briggs DEG. 1979. *Anomalocaris*, the largest known Cambrian arthropod. Palaeontology 22:631–64.

Collins D. 1996. The "evolution" of *Anomalocaris* and its classification in the arthropod Class Dinocarida (nov.) and Order Radiodonta (nov.). J Paleontol 70:280–93.

Daley AC, Bergström J. 2012. The oral cone of *Anomalocaris* is not a classic "*Peytoia*." Naturwisenschaften 99:501–4.

Daley AC, Edgecombe GD. 2014. Morphology of *Anomalocaris canadensis* from the Burgess Shale. J Paleontol 88:68–91.

Di Santo V, Blevins EL, Lauder GV. 2017. Batoid locomotion: effects of speed on pectoral fin deformation in the little skate *Leucoraja erinacea*. J Exp Biol 220:705–12.

Fernando JN, Rival DE. 2016. Reynolds-number scaling of vortex pinch-off on low-aspect ratio propulsors. J Fluid Mech 799:R3.

Figliola RS, Beasley DE. 2011. Theory and design for mechanical measurements. 5th ed. Hoboken (NJ): John Wiley & Sons, Inc.

Gillies JA, Thomas ALR, Taylor GK. 2011. Soaring and manoeuvring flight of a steppe eagle *Aquila nipalensis*. J Avian Biol 42:377–86.

Gursul I, Gordnier R, Visbal M. 2005. Unsteady aerodynamics of nonslender delta wings. Prog Aerosp Sci 41:515–57.

Hou X-G, Bergström J, Ahlberg P. 1995. *Anomalocaris* and other large animals in the Lower Cambrian Chengjiang fauna of southwest China. GFF 117:163–83.

Nedin C. 1999. *Anomalocaris* predation on non-mineralized and mineralized trilobites. Geology 27:987–90.

Paterson JR, García-Bellido DC, Lee MSY, Brock GA, Jago JB, Edgecombe GD. 2011. Acute vision in the giant Cambrian predator *Anomalocaris* and the original of compound eyes. Nature 480:237–40.

Rosenberger LJ. 2001. Pectoral fin locomotion in batoid fishes: undulation versus oscillation. J Exp Biol 204:379–94.

Sfakiotakis L, Lane DM, Davies JBC. 1999. Review of fish swimming modes for aquatic locomotion. IEEE J Ocean Eng 24:237–52.

Thomas ALR. 1993. On the aerodynamics of birds' tails. Philos Trans R Soc Lond B Biol Sci 340:361–80.

Thomas ALR. 1997. On the tails of birds. BioScience 47:215–25.

Tobalske AW. 2007. Biomechanics of bird flight. J Exp Biol 210:3135–46.

Usami Y. 2006. Theoretical study on the body form and swimming pattern of *Anomalocaris* based on hydrodynamic simulation. J Theor Biol 238:11–7.

Usami Y, Saburo H, Inaba S, Kitaoka M. 1998. Reconstruction of extinct animals in the computer. In: Adami C, Belew RK, Kitano H, Taylor C, editors. International conference on artificial life. UCLA: MIT Press. p. 173–7.

Usami Y, Kamono K, Kawamura K. 2003. How *Anomalocaris* swam in the Cambrian sea; a theoretical study based on hydrodynamics. In: Sekimura T, Noji S, Ueno N, Maini PK, editors. Morphogenesis and pattern formation in biological systems: experiments and models. New York (NY): Springer. p. 369–76.

Videler JJ, Wardle CS. 1991. Fish swimming stride by stride: speed limits and endurance. Rev Fish Biol Fish 1:23–40.

Webb PW. 1975. Hydrodynamics and energetics of fish propulsion. Ottawa: Department of the Environment Fisheries and Marine Service.

Webb PW. 2006. Stability and maneuverability. Fish Physiol 23:281–332.

Whittington HB, Briggs DEG. 1985. The largest Cambrian animal, *Anomalocaris*, Burgess Shale, British Columbia. Philos Trans R Soc Lond B Biol Sci 309:569–609.